



# Electrochemical determination of dopamine and uric acid using a glassy carbon electrode modified with a composite consisting of a Co(II)-based metalorganic framework (ZIF-67) and graphene oxide

Jing Tang<sup>1</sup> · Sixun Jiang<sup>1</sup> · Yu Liu<sup>1</sup> · Shengbiao Zheng<sup>1</sup> · Lei Bai<sup>1</sup> · Jiahao Guo<sup>1</sup> · Jianfei Wang<sup>2</sup>

Received: 10 July 2018 / Accepted: 24 September 2018 / Published online: 1 October 2018  
© Springer-Verlag GmbH Austria, part of Springer Nature 2018

## Abstract

A composite was prepared from a Co(II)-based zeolitic imidazolate framework (ZIF-67) and graphene oxide (GO) by an in situ growth method. The material was electrodeposited on a glassy carbon electrode (GCE). The modified GCE was used for the simultaneous voltammetric determination of dopamine (DA) and uric acid (UA), typically at working potentials of 0.11 and 0.25 V (vs. SCE). The morphology and structure of the nanocomposite were characterized by scanning electron microscopy, transmission electron microscopy, Fourier transform infrared spectroscopy and X-ray diffraction. The modified electrode exhibits excellent electroanalytical performance for DA and UA owing to the synergistic effect of the high electrical conductivity of GO and the porosity of ZIF-67. By applying differential pulse voltammetry, a linear response is found for DA in the 0.2 to 80  $\mu\text{M}$  concentration range, and for UA between 0.8 and 200  $\mu\text{M}$ , with detection limits of 50 and 100 nM (at  $S/N = 3$ ), respectively. Further studies were performed on the effect of potential interferents, and on electrode stability and reproducibility. The modified GCE was applied to the simultaneous detection of DA and UA in spiked human urine and gave satisfying recoveries.

**Keywords** Nanocomposite · Scanning electron microscopy · Transmission electron microscopy · Fourier transform infrared spectroscopy · X-ray diffraction · Cyclic voltammetry · Differential pulse voltammetry · Electrochemical sensor · Human urine

## Introduction

Dopamine (DA), an important neurotransmitter, plays an essential role in modulating the brain function. [1]. Uric acid (UA) is the main metabolic product of biological system and the concentration change has been related with various diseases and disorders [2]. Over the past several decades, various

techniques, including capillary electrophoresis [3], spectrophotometry [4], colorimetry [5] and electrochemical methods [6–9], have been applied to the detection of DA and UA. Compared with these above techniques, electrochemical methods have been widely applied since it possesses the merits of high accuracy, fast response, low instrumental and operation expenses [6, 10]. However, there exist some challenges, especially for the very low levels and the interference of coexisting DA and UA in biological samples due to their close oxidation potentials [11]. Thus, electrochemical methods for DA and UA must be developed with suitable modification materials that can provide the separate electrochemical response from those two molecules.

Metal-organic frameworks (MOFs), which are constructed by connecting inorganic metal connectors with organic linkers, have aroused extensive interest by virtue of their exciting properties including large surface areas, high porosity and crystalline nature. These characteristics have made MOFs apply widely in the fields of gas storage [12], catalysis [13], clean energy [14] and sensing [15]. Based on the electrochemical activity of the metal ions and the well-ordered porous

**Electronic supplementary material** The online version of this article (<https://doi.org/10.1007/s00604-018-3025-x>) contains supplementary material, which is available to authorized users.

✉ Jing Tang  
zhengtang102@163.com

✉ Jianfei Wang  
wangjf@ahstu.edu.cn

<sup>1</sup> College of Chemistry and Material Engineering, Anhui Science and Technology University, 1501 Huangshan Road, Bengbu 233000, Anhui Province, China

<sup>2</sup> College of Resource and Environment, Anhui Science and Technology University, Fengyang 233100, Anhui Province, China

skeleton, MOFs have been reported as an electrochemical sensing platform to detect some biomolecules in environmental and industrial applications [16, 17]. Zeolitic imidazolate framework (ZIF-67), as a subclass of metal–organic frameworks, synthesized by assembling cobalt ions ( $\text{Co}^{2+}$ ) and 2-methylimidazole ligands, the large surface areas and the microporous structure of ZIFs have also triggered great interests in the area of electrochemical sensing. Nevertheless, the poor electron-conductive properties of pure MOFs may be the big disadvantage, which would largely limit the application of MOFs in the electrocatalytic process [18]. To resolving this problem, the common strategy is to combining MOFs with the carbon materials which have better electrical conductivity and stability [19].

Among the carbon materials, such as carbon nanofiber, carbon nanotubes, and graphene sheets have been considered as attractive materials in sensing applications due to high surface area, porous structure and high graphitization degree, favourable for the exposure of catalytic active sites, electrocatalysis-related mass transport and electron transfer, respectively [20]. However, SWCNTs film as modified material easily peeled off with the increase of detection times [21]. Graphene oxide stands out as a good candidate modified material for electrochemical analysis [22, 23]. For example, Iqbal et al. [24] have prepared Co-MOF-71 and graphene oxide (GO) composite by hydrothermal method and established an excellent sensor for methanol oxidation reaction. Their study showed that the enhanced electrochemical activity and stability is attributed to the synergetic effect of the MOF and the GO. Wang et al. [25] also demonstrated PDA/ZIF-8@rGO composite was able to immobilization of glucose oxidase to determinate glucose. Moreover, the researchers obtained the fast electron transfer and high electrochemical detection sensitivity because of the synergistic effect of graphene and ZIF-8 crystals. However, the MOF/graphene composites were prepared using physical blend method in that report, which was not stable and effective for electron transfer. Kim et al. have achieved the preparation of graphene/ZIF-67 nanocomposites by in situ growing ZIF-67 on graphene [26].

Inspired by these reports, we have prepared a hybrid nanocomposite of GO-ZIF67 (graphene oxide-zeolitic imidazolate framework-67) by the GO in situ growth of ZIF-67. Then, the GO-ZIF67 modified glassy carbon electrode was fabricated by the electrodeposition method and applied for the determination of DA and UA simultaneously. The combination way of GO and ZIF-67 was very simple, and made the modified electrode more stable in the actual detection. Compare with drop casting method, the GO-ZIF67/GCE by electrodeposition method have more stability and better electrochemical performance for DA and UA. An enhanced electrocatalytic performance of this modified electrode have been received due to the excellent conductivity of GO and the porous structure and large surface area of MOF. Therefore, this

work gives help for using GO-ZIF67 composites for the electrochemical sensing.

## Experimental

### Reagents

Graphite was provided by XFNANO Materials Tech Co., Ltd. (Nanjing China, <https://www.xfnano.com>). 2-methylimidazole,  $\text{Co}(\text{NO}_3)_2 \cdot 6\text{H}_2\text{O}$ , uric acid (UA), dopamine (DA) and  $\text{KMnO}_4$  were obtained from Aladdin Chemical Reagent Co. Ltd. (Shanghai China, <http://www.aladdin-e.com>). 0.1 M phosphate buffer with different pH values were prepared by mixing the solutions of  $\text{NaH}_2\text{PO}_4 \cdot 2\text{H}_2\text{O}$  and  $\text{Na}_2\text{HPO}_4 \cdot 12\text{H}_2\text{O}$ , and then adjusting the pH with  $\text{H}_3\text{PO}_4$  or  $\text{NaOH}$ . All the reagents were of analytical grade and used as such without purification. Double-distilled water (resistivity  $>18 \text{ M}\Omega \cdot \text{cm}$ ) was used throughout all experiments.

### Apparatus

The electrochemical experiments, including cyclic voltammetry (CV) and differential pulse voltammetry (DPV) were conducted on a CHI-660E electrochemical analyzer (Shanghai Chenhua Instruments, China, <http://www.chinstr.com>) with conventional three-electrode system. A bare or modified glassy carbon electrode (GCE, 3 mm in diameter) was employed as the working electrode. Platinum wire and saturated calomel electrodes were used as the auxiliary and reference electrodes, respectively. Electrochemical impedance spectroscopy (EIS) was carried out using Princeton PARSTAT4000 (<http://www.par-solartron.com>) between 0.1 Hz and 10 kHz at 0.25 V. Scanning electron microscopy (SEM) images were obtained by EVO18 (Carl Zeiss, German, <https://www.zeiss.com>). Transmission electron microscopy (TEM) images were obtained by JEOL JEM-2100 (Japan, <http://www.starjoy-china.com>). Energy-dispersive X-ray spectroscopy (EDX) was recorded using a BRUKER quantax 200 (German, <https://www.bruker.com>). X-ray diffraction (XRD) was operated on a Rigaku Ultima IV diffractometer (Japan, <https://www.rigaku.com>). FT-IR spectra were recorded on a Thermo Fisher FT-IR spectrometer (USA, <https://www.thermofisher.com>).

### Preparation of GO, ZIF-67 and GO-ZIF67

Graphene oxide was prepared by Hummers' method [27]. ZIF-67 was synthesized according to the literature [28] and the preparation details were deposited in the

electronic supporting material. The GO-ZIF67 nanocomposite was synthesized by the GO growth of ZIF-67 [26] (Scheme 1). First, GO (60 mg) were dispersed in methanol (25 mL) and sonicated for 4 h.  $\text{Co}(\text{NO}_3)_2 \cdot 6\text{H}_2\text{O}$  (293 mg) was added and stirred for another 4 h. 2-methylimidazole (328 mg) was dissolved in another methanol (25 mL). Then the solution was poured to the mixture of GO and  $\text{Co}(\text{NO}_3)_2 \cdot 6\text{H}_2\text{O}$  solution and under vigorous stirring for 6 h. The dark purple precipitates were collected by centrifugation with  $2451\times g$  and wash with 50 mL of methanol at least three times to remove any leftover precursor. Finally, the samples were dried in a vacuum oven at  $60^\circ\text{C}$  for 24 h to obtain the GO-ZIF67 nanocomposite.

### Fabrication of GO-ZIF67 modified electrode

Prior to the modification, the GCE was polished with aqueous slurries of alumina (0.3 and  $0.05\ \mu\text{m}$ ) and then successively ultrasonically cleaned in anhydrous alcohol and double distilled water and dried by nitrogen for further use. Next, the GO-ZIF67 composite was dispersed ultrasonically in the DMF containing 0.1 M  $\text{NaNO}_3$  to form  $1.0\ \text{mg}\cdot\text{mL}^{-1}$  GO-ZIF67 suspension. The electrodeposition of GO-ZIF67 on GCE was carried out by CV in the range of  $-1.0$  to  $1.5\ \text{V}$  at a scan rate of  $100\ \text{mV}\cdot\text{s}^{-1}$  for 25 cycles. The modified electrode was donated as GO-ZIF67/GCE. As controls, GO/GCE and ZIF-67/GCE were also prepared through the same conditions in the respective solutions. The electrodes

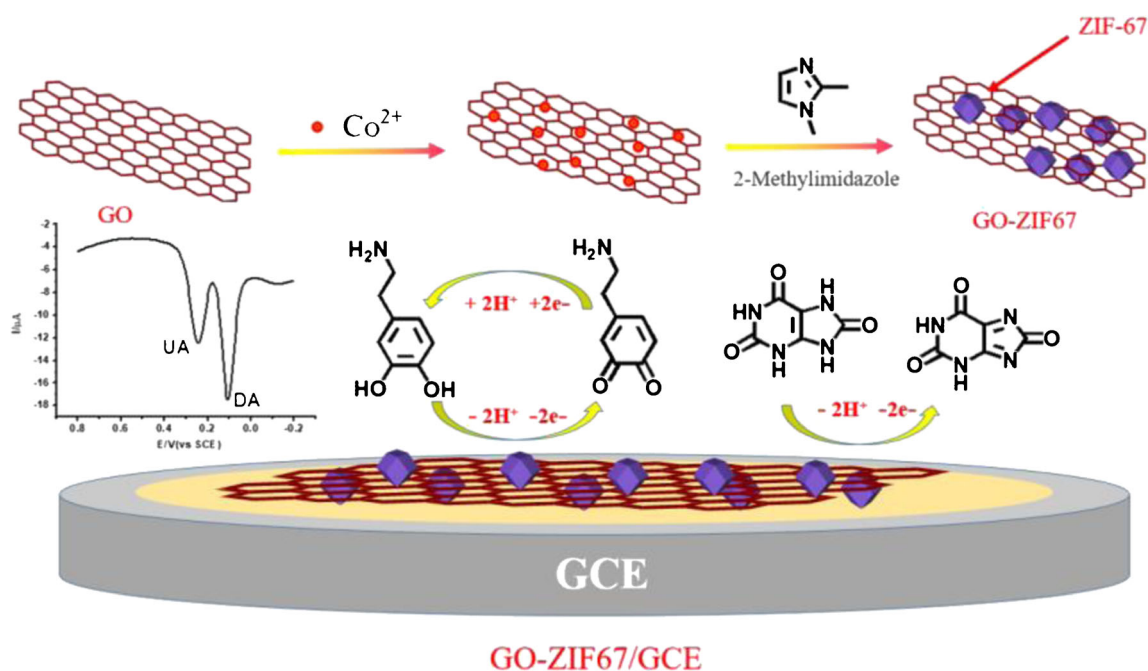
were rinsed with deionized water and dried by nitrogen before used for experiments.

### Electrochemical measurements

The CV experiments were performed in phosphate buffer (pH = 7.4) containing appropriate amounts of DA and UA. DPV was recorded within the potential range from  $-0.2\ \text{V}$  to  $+0.6\ \text{V}$  with a pulse amplitude  $50\ \text{mV}$ , pulse width  $50\ \text{ms}$  in phosphate buffer. The electrode was electrochemically subjected to potential cycling between  $-0.8$  and  $0.8\ \text{V}$  in phosphate buffer (pH 7.4) at  $100\ \text{mV}\cdot\text{s}^{-1}$  until a steady state was reached for next experiment. The electrochemical behaviors of the electrodes were performed by EIS in  $5.0\ \text{mM}\ \text{Fe}(\text{CN})_6^{3-/4-}$  solution containing  $0.1\ \text{M}\ \text{KCl}$  solution with the frequency between  $0.1$  and  $10\ \text{kHz}$ . All the electrochemical experiments were carried out at room temperature.

### Sample analysis

Human urine samples were supplied by healthy volunteers. The human urine samples ( $1\ \text{mL}$ ) were respectively diluted 50 times (by volume) with phosphate buffer (pH = 7.4) without any sample pretreatment and analyzed by DPV. The peak currents of the analytes were recorded at a potential of  $0.25\ \text{V}$  and their concentrations were determined. Recovery tests were conducted by adding known amounts of DA and UA to the urine samples by DPV.



**Scheme 1** Preparation procedure of GO-ZIF67 and electrochemical reaction mechanisms of UA and DA at the GO-ZIF67/GCE

## Results and discussion

### Choice of materials

ZIF-67 has the microporous structure as well as the large surface areas for the electrochemical reaction of DA and UA. This results in a high current response for DA and UA molecule detection. The incorporation of ZIF-67 overcomes the aggregation of the graphene oxide and thus greatly improves the surface area of the GO-ZIF67 composites. The properties of GO such as high surface area, good flexibility and excellent chemical stability are particularly useful to anchor various functional nanomaterials in the preparation of a hybrid structure. The improved conductivity of ZIF-67 provided by nanomaterials incorporated. In addition, the interference from AA when determining DA and UA can partly be avoided by modifying the electrode surface with the negatively charged carboxylate groups on the GO. The electrochemical response to DA and UA detection are greatly affected by synergistic effects of the composite. So, the GO-ZIF67 was selected as the platform for the determination of DA and UA.

### Characterization of GO-ZIF67, GO and ZIF-67

The prepared of GO-ZIF67, GO and ZIF-67 were characterized by XRD, FT-IR, SEM and TEM. The XRD patterns of them are displayed in Fig. 1a. The standard diffraction patterns of simulated GO and ZIF-67 are also provided for comparison. For GO, a diffraction peak was located at  $2\theta = 8.0^\circ$ , belongs to the (001) crystal planes of GO spectrum, which was consistent with the previous characteristics of GO [29]. The peaks ascribed to the synthesized ZIF-67 matched well with simulated sample, which confirmed the purity ZIF-67 was successfully fabricated. The pattern of GO-ZIF67 composite was similar to that of ZIF-67, which indicated that the structure of ZIF-67 was largely preserved in the composite samples.

FT-IR spectra can give the information on the functional groups and structural properties (Fig. 1b). For GO, typical GO peaks such as O-H peak at  $3400\text{ cm}^{-1}$ , C=O peak at around

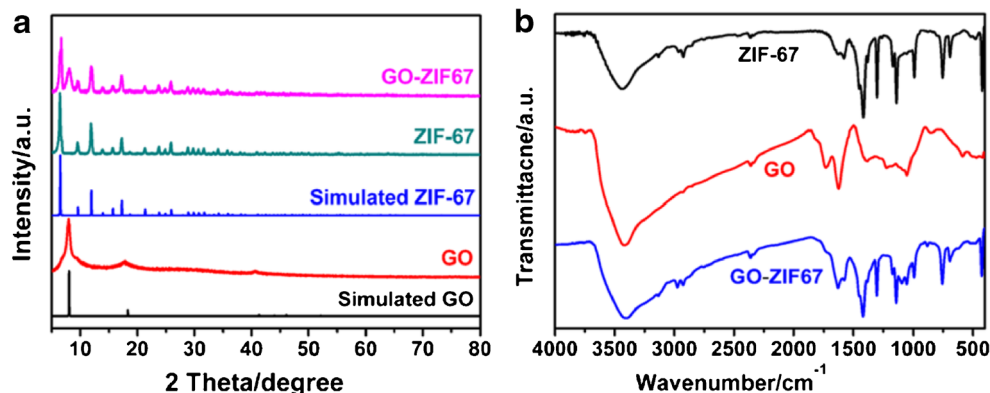
$1730\text{ cm}^{-1}$ , C-O-H peak at  $1600\text{ cm}^{-1}$ , C-O peak at  $1410\text{ cm}^{-1}$  and C-O peak at  $1200\text{ cm}^{-1}$  were observed [30]. As for ZIF-67, the peaks in the range of  $600\text{--}1500\text{ cm}^{-1}$  from the stretching and bending modes of the imidazole ring, the peak at  $1584\text{ cm}^{-1}$  can be assigned as the C=N stretch mode in 2-methylimidazole, and the peaks at  $2930$  and  $3145\text{ cm}^{-1}$  attributed to the stretching mode of C-H from the aromatic ring and the aliphatic chain [31]. For GO-ZIF67, both characteristic peaks from ZIF-67 and GO can be found in GO-ZIF67, showing that compositions of ZIF-67 and GO were preserved after the synthesized process.

Figure 2a displays the SEM image of GO, the obvious wrinkles in the rigid structures were observed in accordance with the reported literature [29]. The EDX spectrum of GO is depicts in Fig. 2d, the elements C and O were detected, conforming the formation of GO. The SEM image of ZIF-67 showed a typical polyhedral morphology with a particle size of  $400\text{--}500\text{ nm}$  (Fig. 2b). From the SEM image of GO/ZIF-67 composite (Fig. 2c), the translucent GO which were blending with ZIF particles can be observed, which revealed the anchoring and growth of ZIF-67 nanocrystals on the GO surfaces. The transmission electron microscopy (TEM) was employed to investigate the nanostructure of GO and GO-ZIF67 composite. Figure 2e and f were the TEM images of GO (e) and GO-ZIF67 composite (f), it exhibited the translucent GO which are blending with ZIF particles, providing large specific surface area.

### Characterization of modified electrodes

The electrodeposition of ZIF-67, GO and GO-ZIF67 composite on the GCE surface was performed by CV. The morphologies of different materials on the GCE surface were investigated by SEM. Fig. S1a showed that GO was homogeneously coated on the surface of the electrode. EDX measurement was performed to validate the presence of GO (Fig. S1d). Fig. S1b showed the surface of ZIF-67/GCE, the ZIF-67 crystal particles aggregated and polyhedral morphology. The corresponding EDX spectrum of the deposited microstructures is shown in Fig. S1e. After the deposition of GO-ZIF67, it can be seen

**Fig. 1** a X-ray diffraction patterns of GO, ZIF-67 and GO-ZIF67, b FT-IR spectra of GO, ZIF-67 and GO-ZIF67



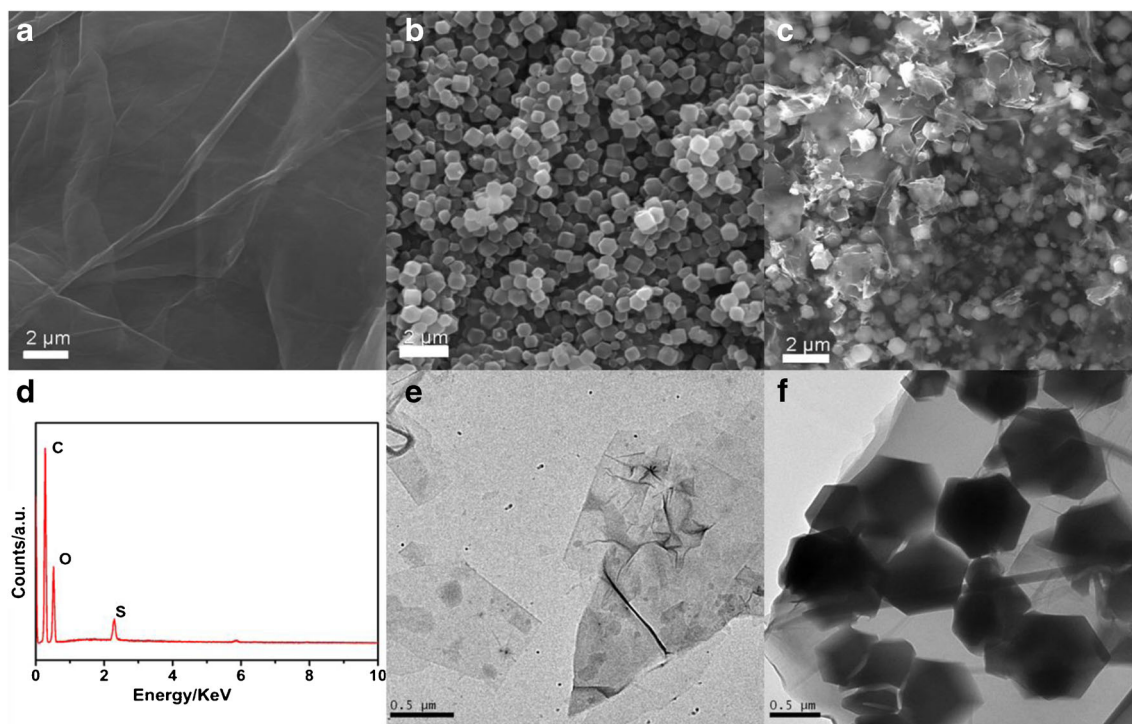


**Fig. 2** SEM images of GO (a), ZIF-67 (b), GO-ZIF67 composite (c), (d) EDX spectrum of GO, TEM images of the GO (e) and GO-ZIF67 composite (f)

from Fig. S1c that ZIF-67 crystals were homogeneously grown on the surface of GO, implying that the high accessible surface area and thus the high sensitivity by using in sensor for detection. The EDX spectrum of GO-ZIF67 is depicts in Fig. S1f C, O, Co and N were detected.

Electrochemical properties of the different electrodes were characterized by  $K_3[Fe(CN)_6]$  as a probe by cyclic voltammetry. Fig. S2 shows the cyclic voltammograms of bare GCE, GO/GCE, ZIF-67/GCE and GO-ZIF67/GCE in 5.0 mM  $[Fe(CN)_6]^{3-/4-}$  containing 0.1 M KCl. The  $I_{pa}$  (about  $9.79 \times 10^{-4} \text{ A}\cdot\text{cm}^{-2}$ ) achieved at GO-ZIF67/GCE was found almost 2-fold larger than that achieved at bare GCE due to the larger surface area and good conductivity of GO-ZIF67 composite modified electrode. For a reversible process, the peak current ( $I_p$ ) increased linearly proportional to the square root of scan rates ( $v^{1/2}$ ) as follows (the Randles-Sevcik formula):

$$I_p = 2.69 \times 10^5 n^{3/2} A D_0^{1/2} C_0 v^{1/2}$$

where  $I_p$  is the peak current,  $n$  is the number of electrons involved ( $n = 1$  in the  $[Fe(CN)_6]^{3-/4-}$  redox system),  $A$  is the surface area of electrode,  $C_0$  is the concentration of the reactant,  $D_0$  is the diffusion coefficient of the  $[Fe(CN)_6]^{3-/4-}$  ( $6.7 \times 10^{-6} \text{ cm}^2\cdot\text{s}^{-1}$ ) and  $v$  is the scan rate. Thus, from the slope of the anodic peak current ( $I_{pa}$ ) versus square root of scan rate ( $v^{1/2}$ ) relation (inset of Fig. S2), the value of  $A$  for GO-ZIF67/GCE was  $0.100 \text{ cm}^2$ , which was larger than that of ZIF-67/GCE ( $0.085 \text{ cm}^2$ ), GO/GCE ( $0.078 \text{ cm}^2$ ) and bare GCE ( $0.052 \text{ cm}^2$ ), indicating that the effective electroactive surface

of the modified electrode was increased in the presence of ZIF-67 and GO.

In order to investigate the electron charge property of modified electrodes, EIS was carried out by the use of the redox couple probe  $Fe(CN)_6^{3-/4-}$  in the solution of 5 mM  $Fe(CN)_6^{3-/4-}$  containing 0.1 M KCl, as shown in Fig. 3. The diameter of semicircular element at higher frequencies corresponded to

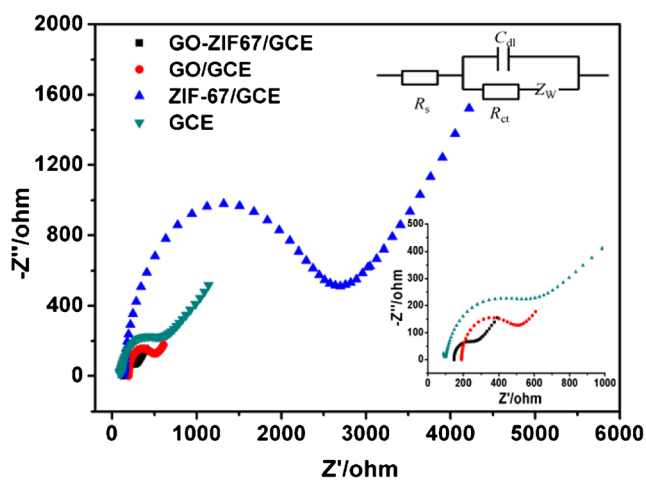


**Fig. 3** Nyquist plots of different electrodes in 5 mM  $[Fe(CN)_6]^{3-/4-}$  containing 0.1 M KCl. Frequency range: 10 kHz to 0.1 Hz; potential: 0.25 V. Inset: the Randle equivalent circuit applied to fit the data and the enlargement of the plots of bare GCE, GO/GCE and GO-ZIF67/GCE. The Randles equivalence circuit included the electrolyte resistance ( $R_s$ ), Warburg impedance ( $Z_w$ ), charge transfer resistance ( $R_{ct}$ ) and double layer capacitance ( $C_{dl}$ )

the electron transfer resistance ( $R_{ct}$ ) between electrode surface and  $\text{Fe}(\text{CN})_6^{3-/4-}$ , while the linear part at lower frequency represented the diffusion process. The nyquist curve of the bare GCE had an obviously semicircle in high frequency region, indicating a poor interfacial electron transfer. The diameter of the semicircle significantly increased after being introduced ZIF-67, which is ascribed to the modification of poor conductive ZIF-67 at GCE. However, the diameter of the semicircle of the GO/GCE markedly decreased because of its good stability and electrical conductivity. The semicircle was smallest than other electrodes when GO-ZIF67 composite modified on electrode surface, which can be ascribed to cooperative action between GO and ZIF-67, suggesting that poor conductivity of ZIF-67/GCE can be overcome by the incorporation of the GO. This result indicated that high interfacial electron transfer take place at the GO-ZIF67/GCE.

### Electrochemical behavior to DA and UA at the GO-ZIF67/GCE

The electrochemical behaviors of DA and UA at different modified electrodes were studied in the phosphate buffer (pH 7.4) using CV method and the results were shown in Fig. 4a, b and c. As shown in Fig. 4a, an irreversible redox

couple for DA with small current height (only  $11 \mu\text{A}\cdot\text{cm}^{-2}$ ) was observed at the bare GCE. While for GO,  $\Delta E_p$  was remarkably reduced, indicating that GO/GCE had a better electrocatalytic activities and a fast electron transfer for DA. When the ZIF-67 was introduced, a pair of well-defined redox couple for DA was observed with large increase of current height (about  $99 \mu\text{A}\cdot\text{cm}^{-2}$ ) due to the great surface area and the porosity of ZIF-67. GO-ZIF67/GCE (curve d) did not shift the oxidation and reduction potential of DA but it increased the oxidation currents of DA. These results obviously demonstrated that GO and ZIF-67 composite can enhance the oxidation of DA on the GO-ZIF67/GCE attributing to the synergistic effects of the porosity of ZIF-67 and the superior electric conductivity of GO. Similarly, for UA the oxidation peak potential was shifted to the less negative potential with large increase of current height when bare GCE, GO/GCE, ZIF-67/GCE and GO-ZIF67/GCE was used successively (Fig. 4b). As shown in Fig. 4c, in the same case, two well-defined oxidation peaks corresponding to DA and UA (a separation of 140 mV in oxidation peak currents) were received in DA and UA mixtures and the oxidation peak currents of them detected by GO-ZIF67/GCE were significantly higher than the peak currents of other electrodes. The distinguishable electrochemical signals at the GO-ZIF67/GCE provided the favorable

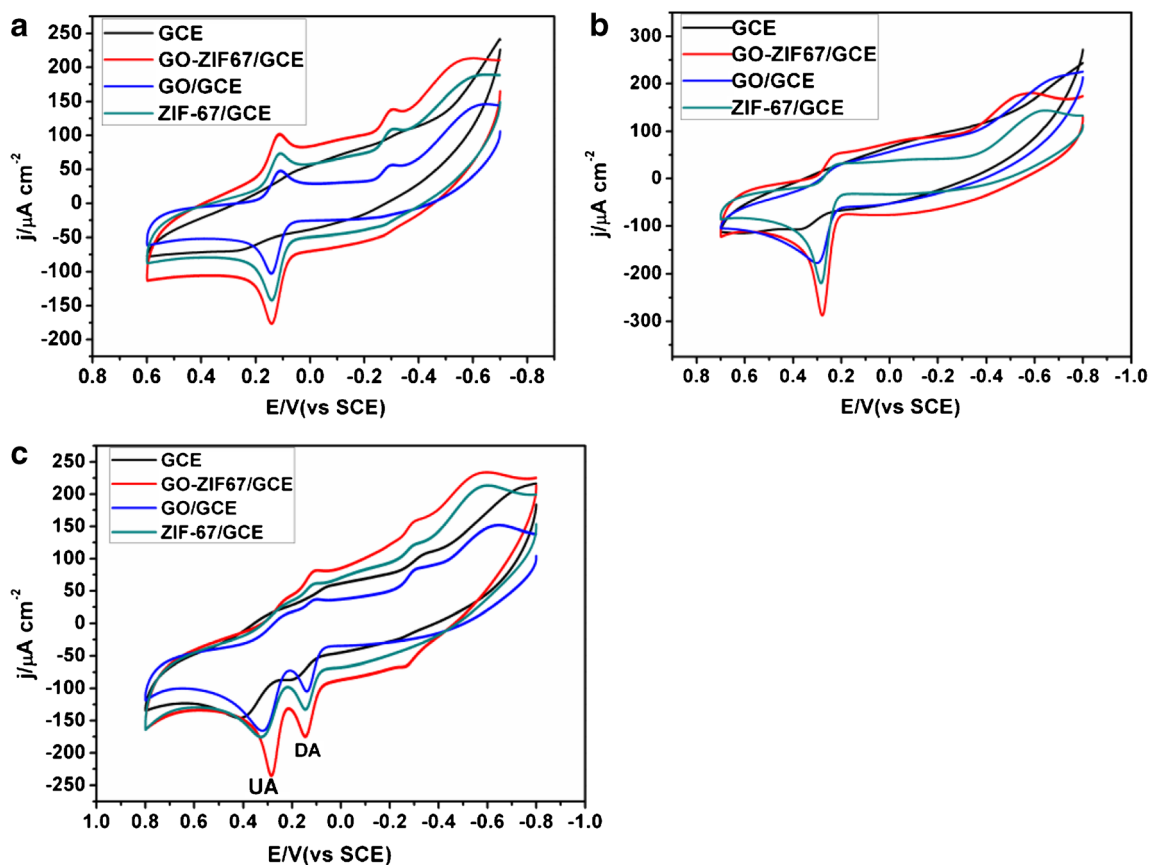


**Fig. 4** CVs of 100  $\mu\text{M}$  of DA (a), 200  $\mu\text{M}$  UA (b) and a mixture of 100  $\mu\text{M}$  DA and 200  $\mu\text{M}$  UA (c) at the different modified electrodes based on GCE, GO/GCE, ZIF-67/GCE and GO-ZIF67/GCE in phosphate buffer (pH 7.4) at scan rate:  $100 \text{ mV}\cdot\text{s}^{-1}$

possibility for the effectively and simultaneous determination of DA and UA. Otherwise, compare the two preparation methods, DPV of the mixture solutions of DA and UA in phosphate buffer at GO-ZIF67 modified electrode by electrodeposition and drop casting is shown in Fig. S3. The result suggested that the GO-ZIF67/GCE by the electrodeposition method have the less negative potential and larger increase of current response for DA and UA than by the drop casting method.

To further investigate the reaction of DA and UA at the GO-ZIF67/GCE, the effect of the scan rate on their electrochemical responses were studied by CV. As shown in Fig. S4, the peak currents ( $I$ ) of DA and UA increased with the augment of scan rates and they accurately followed a linear relationship between peak currents and the square root of scan rates over the range of 20 to 400  $\text{mV}\cdot\text{s}^{-1}$ . In addition, the linear regression equation for DA of  $I_{pa} (\mu\text{A}\cdot\text{cm}^{-2}) = -286.75v^{1/2} + 3.124$  ( $v$  in  $\text{V}\cdot\text{s}^{-1}$ ), with a correlation coefficient of  $R = 0.990$ ,  $I_{pc} (\mu\text{A}\cdot\text{cm}^{-2}) = 252.4v^{1/2} - 32.95$  ( $v$  in  $\text{V}\cdot\text{s}^{-1}$ ), with a correlation coefficient of  $R = 0.978$  and for UA of  $I_{pa} (\mu\text{A}\cdot\text{cm}^{-2}) = -418.35v^{1/2} - 1.920$  ( $v$  in  $\text{V}\cdot\text{s}^{-1}$ ), with a correlation coefficient of  $R = 0.998$ , were extracted, respectively. This indicated that the diffusion process was a controlling factor to impact the

electrochemical response of DA and UA and the fast electron-transfer process of DA and UA at this modified electrode [8].

### Optimization of method

In order to achieve the optimum results, the following parameters were optimized: (a) Sample pH value and (b) number of scans for the electrodeposition of the modifier. The respective data and figures are presented in the electronic supporting material (Fig. S5). In short, the following experimental conditions were found to give best results: (a) Best sample pH value: 7.4; (b) Optimal scans: 25.

### Simultaneous determination of DA and UA

The simultaneous and quantitative determination of UA and DA at GO-ZIF67/GCE were studied by DPV because of its high current sensitivity and good resolution. Figure 5 shows the DPVs recorded for various concentrations of DA and UA, respectively, in the presence of constant concentrations of another part (100  $\mu\text{M}$  UA and 50  $\mu\text{M}$  DA). As shown in Fig. 5a, the anodic peak current was proportional to the concentration

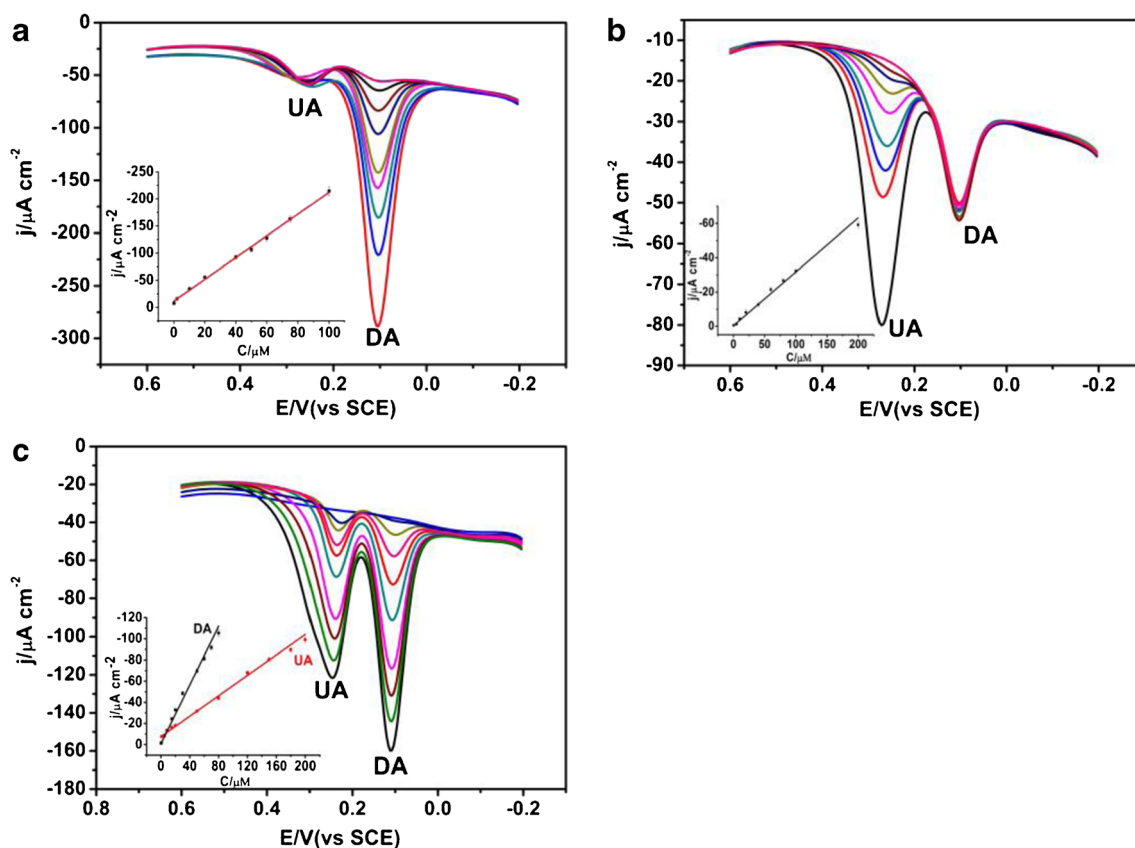


**Fig. 5** Differential pulse voltammetry of GO-ZIF67/GCE in phosphate buffer (pH 7.4) **a** Containing 80  $\mu\text{M}$  UA and different concentrations of DA from 0.1 to 100  $\mu\text{M}$  **b** Containing 10  $\mu\text{M}$  UA and different concentrations of UA from 0.5 to 200  $\mu\text{M}$  **c** Simultaneous DPV

determination of DA (0.2–80  $\mu\text{M}$ ) and UA (0.8–200  $\mu\text{M}$ ). Inset: Variation of the DPV oxidation peak currents against their concentration for DA (inset of 5a), UA (inset of 5b) and mixture of DA and UA (inset of 5c), respectively. Pulse time: 50 ms, potential step: 50 mV

**Table 1** Comparison of analytical performances at different materials-based electrochemical sensors for the simultaneous electrochemical determination of DA and UA

Materials	Linear range ( $\mu\text{M}$ )		Detection limit ( $\mu\text{M}$ )		Reference
	DA	UA	DA	UA	
mp-GR <sup>a</sup>	4–40	5–120	1.5	2.0	[8]
GNP/ch <sup>b</sup>	0.2–80	1.2–100	0.12	1.6	[10]
ANF-C70C <sup>c</sup>	1–80	1–60	0.47	0.28	[32]
H-Fe <sub>3</sub> O <sub>4</sub> @C/GNS <sup>d</sup>	0.1–150	1.0–100	0.053	0.41	[33]
p-ATD <sup>e</sup>	5–50	10–100	0.33	0.19	[34]
$\beta$ -CD/CQDs <sup>f</sup>	4–220	0.3–200	0.14	0.01	[35]
GO-ZIF67	0.2–80	0.8–200	0.05	0.1	This work

<sup>a</sup>: multi-nanopore graphene; <sup>b</sup>: gold nanoparticle/choline; <sup>c</sup>: alumina nanofibers; <sup>d</sup>: graphene oxide nanosheet; <sup>e</sup>: poly(2-amino-1,3,4-thiadiazole); <sup>f</sup>: poly( $\beta$ -cyclodextrin)/carbon quantum dots

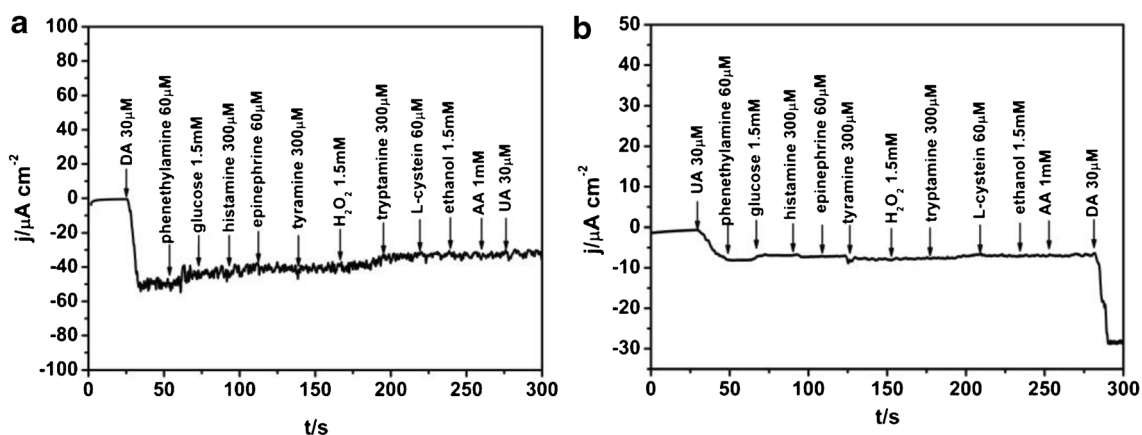
of DA while the peak current of UA almost kept constant, the peak currents linearly increased with increasing concentration of DA in the range of 0.1  $\mu\text{M}$ –100  $\mu\text{M}$ . The regression equation was  $I_{pa} (\mu\text{A}\cdot\text{cm}^{-2}) = -2.000C (\mu\text{M}) - 11.61$  ( $R = 0.9958$ ) with the detection limit (LOD) of 0.02  $\mu\text{M}$  ( $S/N = 3$ ), sensitivity was 2.000  $\mu\text{A}\cdot\mu\text{M}^{-2}\cdot\text{cm}^{-2}$ . Similar patterns were observed for UA with respect to DA (Fig. 5b), the anodic peak current of UA was proportional to the concentration from 0.5  $\mu\text{M}$  to 200  $\mu\text{M}$  ( $R = 0.9996$ ) with a regression equation of  $I_{pa} (\mu\text{A}\cdot\text{cm}^{-2}) = -0.314C (\mu\text{M}) - 0.300$  ( $R = 0.9925$ ) and the LOD was 0.1  $\mu\text{M}$  ( $S/N = 3$ ), sensitivity was 0.314  $\mu\text{A}\cdot\mu\text{M}^{-2}\cdot\text{cm}^{-2}$ , indicating that the oxidation of DA and UA at GO-ZIF67 modified electrode took place independently without any mutual interference.

Figure 5c shows DPV curves of DA and UA in the mixture solution by simultaneously changing their concentrations. The oxidation peak current ( $I_{pa}$ ) were proportional to their concentrations from 0.2  $\mu\text{M}$  to 80  $\mu\text{M}$  for DA and from 0.8  $\mu\text{M}$  to 200  $\mu\text{M}$  for UA. Inset in Fig. 5c shows the regression equations were  $I_{pa} (\mu\text{A}\cdot\text{cm}^{-2}) = -1.387C (\mu\text{M}) - 0.882$  ( $R = 0.9923$ ) for DA and  $I_{pa} (\mu\text{A}\cdot\text{cm}^{-2}) = -0.482C (\mu\text{M}) - 7.538$  ( $R = 0.9912$ ) for UA, respectively. And the detection limits for DA and UA were estimated to be 0.05  $\mu\text{M}$  and 0.1  $\mu\text{M}$

( $S/N = 3$ ), respectively. The sensitivity for DA and UA were 1.387  $\mu\text{A}\cdot\mu\text{M}^{-2}\cdot\text{cm}^{-2}$  and 0.482  $\mu\text{A}\cdot\mu\text{M}^{-2}\cdot\text{cm}^{-2}$ , respectively. These results suggested that the GO-ZIF67/GCE can be successfully used for simultaneous determination of DA and UA without interference with each other. Table 1 summarizes the comparison of the GO-ZIF67 modified electrode with other modified electrodes for simultaneous detection of DA and UA. It showed that this modified electrode in the present work has a low detection limit and wide linear range. The enhanced electrocatalytic performances of the GO-ZIF67/GCE may be attributed to the synergistic effects of GO and ZIF-67. The nanocomposite combine the great electric conductivity of GO, large specific surface area and ordered pore structure of ZIF-67, which promote the electron transfer.

### Selectivity, stability and reproducibility

Resistance to interference is an important parameter for an electrochemical sensor. AA is one of major interfering species affecting electrochemical DA and UA detection in the analysis of real samples. Fig. S6 shows DPV curve of a mixture of DA, UA and AA at the GO-ZIF67/GCE. The high concentration of



**Fig. 6** Amperometric responses of GO-ZIF67/GCE upon addition of 30  $\mu\text{M}$  of DA, UA, and other interfering chemicals to phosphate buffer (pH 7.4) at applied potential of 0.11 V (a) and 0.25 V (b) vs SCE under a constant-rate stirring condition



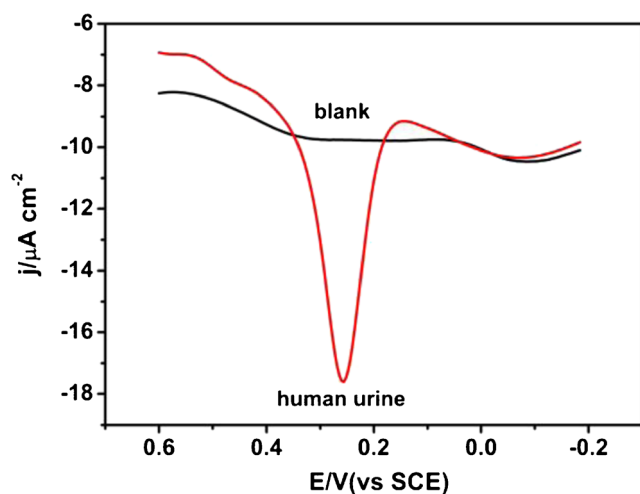


**Fig. 7** Typical DPVs at GO-ZIF67/GCE in phosphate buffer (pH 7.4) in the absence and presence of human urine, Pulse time: 50 ms, potential step: 50 mV

AA exhibited a poor electrochemical response on GO-ZIF67/GCE and the separation of the oxidation peak potentials of those analytes were large enough for distinguish. It may be attributed to the electrostatic repulsion due to the negatively charged carboxylate groups on the GO, which exclude most of the AA anions from the surface of the electrode. Figure 6a shows the current responses of the GCE to DA and a series of possible interference. There is obvious current response with the addition of 30  $\mu\text{M}$  DA. Insignificant interferences (signal change <5%) observed was observed for the following compounds: L-cystein, AA, epinephrine, histamine, glucose, hydrogen peroxide ( $\text{H}_2\text{O}_2$ ), ethanol, tyramine, tryptamine and phenethylamine. At a potential of 0.25 V (Fig. 6b), no current response was observed with the addition of these interfering species. All results show good selectivity of the GCE.

The stability of GO-ZIF67/GCE was evaluated in the mixed solution containing 10  $\mu\text{M}$  DA and 50  $\mu\text{M}$  UA. The oxidative currents of this method had a relative standard deviation (*RSD*) for DA and UA in seven successive measurements was 2.56 and 2.12%, respectively,

**Table 2** Determination of DA and UA in human urine samples on GO-ZIF67/GCE ( $n = 5$ )

Sample	Analyte	Detected ( $\mu\text{M}$ )	Added ( $\mu\text{M}$ )	Found <sup>a</sup> ( $\mu\text{M}$ )	RSD <sup>b</sup> (%)	Recovery (%)
1	DA	ND <sup>c</sup>	10	10.39 $\pm$ 0.15	1.44	103.9
	UA	2.53	10	12.61 $\pm$ 0.12	0.95	100.6
2	DA	ND	20	19.64 $\pm$ 0.22	1.12	98.2
	UA	1.61	20	21.02 $\pm$ 0.13	0.62	97.3
3	DA	ND	30	29.27 $\pm$ 0.17	0.58	97.6
	UA	1.80	30	31.49 $\pm$ 0.16	0.51	99.0

<sup>a</sup> Standard addition method

<sup>b</sup> Relative standard deviation for 5 successive measurements

<sup>c</sup> ND: not detected

indicating an excellent stability. The reproducibility of the sensor was tested by using four different modified electrodes, the *RSD* was 4.78 and 3.06% for DA and UA, respectively. Thus, the GO-ZIF67/GCE has good reproducibility along with a considerable average stability towards simultaneous determination of DA and UA. However, this modified electrode indeed has some limitations, especially unfavorable long-time stability. The GO-ZIF67/GCE was stored at 4  $^{\circ}\text{C}$  for 10 days when not in use; the peak current decreased to about 85% of its initial value with the concentration of 10  $\mu\text{M}$  DA and 50  $\mu\text{M}$  UA. It may be mainly due to storage conditions. The long-time stability can be improved with improvement of storage conditions.

## Analytical applications

For the evaluation of this method in real samples, the GO-ZIF67/GCE was applied to the determination of DA and UA in human urine by using the standard addition method. DPVs of phosphate buffer (pH 7.4) in the absence and presence of human urine sample are shown in Fig. 7. A large increase in peak current was obtained at a potential of 0.25 V, indicating that UA was in the urine sample. The determination of each species was measured by DPV and detection results are summarized in Table 2. The recoveries were 97.6–103.9% for DA and 97.3–100.6% for UA, respectively, confirming the modified electrodes have the potential to simultaneously determine DA and UA in biomedical samples.

## Conclusions

In summary, a novel modified glassy carbon electrode (GCE) was fabricated by electrodeposition using graphene oxide and ZIF-67 nanocomposite. The GO-ZIF67/GCE exhibited good electroactivity to the oxidation of DA and UA. The GO-ZIF67 modified electrode was utilized for the simultaneous determination of DA and UA and the oxidation peak potentials exhibited sharp differences between DA and UA with good

sensitivity and selectivity. The GCE showed good analytical parameters (including detection limit and linear range) that can be due to the synergistic effect between GO and ZIF-67. Moreover, the GCE was successfully used for the detection of DA and UA in the human urine, showing its promising application in real samples analysis.

**Acknowledgements** This work was supported by the National Nature Foundation of Anhui Province (Grants 1808085 MB31), the Project of Education Department of Anhui Province (KJ2017A506), the key discipline of Anhui Science and Technology University (AKZDXK2015A01) and the Student's Platform for Innovation and Entrepreneurship Training Program of China (201810879020).

**Compliance with ethical standards** The author(s) declare that they have no competing interests.

## References

- Kim YR, Bong S, Kang YJ, Yang Y, Mahajan RK, Kim JS, Kim H (2010) Electrochemical detection of dopamine in the presence of ascorbic acid using graphene modified electrodes. *Biosens Bioelectron* 25:2366–2369
- Ndamanisha JC, Guo L (2004) Electrochemical determination of uric acid at ordered mesoporous carbon functionalized with ferrocenecarboxylic acid-modified electrode. *Biosens Bioelectron* 23:1680–1685
- Pormsila W, Krähenbühl S, Hauser PC (2009) Capillary electrophoresis with contactless conductivity detection for uric acid determination in biological fluids. *Anal Chim Acta* 636:224–228
- Moghadam MR, Dadfarnia S, Shabani AMH, Shahbazikhah P (2011) Chemometric-assisted kinetic-spectrophotometric method for simultaneous determination of ascorbic acid, uric acid, and dopamine. *Anal Biochem* 410:289–295
- Tao Y, Lin YH, Ren JS, Qu XG (2013) A dual fluorometric and colorimetric sensor for dopamine based on BSA-stabilized Au nanoclusters. *Biosens Bioelectron* 42:41–46
- Sheng ZH, Zheng XQ, Xu JY, Bao WJ, Wang FB, Xia XH (2012) Electrochemical sensor based on nitrogen doped graphene: simultaneous determination of ascorbic acid, dopamine and uric acid. *Biosens Bioelectron* 34:125–131
- Tian FY, Li HJ, Li MJ, Li CP, Lei YJ, Yang BH (2017) A tantalum electrode coated with graphene nanowalls for simultaneous voltammetric determination of dopamine, uric acid, L-tyrosine, and hydrochlorothiazide. *Microchim Acta* 184:1611–1617
- Zhu XH, Liang Y, Zuo XX, Hu RP, Xiao X, Nan JM (2014) Novel water-soluble multi-nanopore graphene modified glassy carbon electrode for simultaneous determination of dopamine and uric acid in the presence of ascorbic acid. *Electrochim Acta* 143:366–373
- Dey MK, Satpati AK (2017) Functionalised carbon nano spheres modified electrode for simultaneous determination of dopamine and uric acid. *J Electroanal Chem* 787:95–102
- Wang P, Li YX, Huang X, Wang L (2007) Fabrication of layer-by-layer modified multilayer films containing choline and gold nanoparticles and its sensing application for electrochemical determination of dopamine and uric acid. *Talanta* 73:431–437
- Prathap MUA, Srivastava R (2013) Tailoring properties of polyaniline for simultaneous determination of a quaternary mixture of ascorbic acid, dopamine, uric acid, and tryptophan. *Sensors Actuators B Chem* 177:239–250
- Dinca M, Long JR (2008) Hydrogen storage in microporous metal-organic frameworks with exposed metal sites. *Angew Chem Int Ed Engl* 47:6766–6779
- Cui L, Wu J, Li J, Ju H (2015) Electrochemical sensor for lead cation sensitized with a DNA functionalized porphyrinic metal-organic framework. *Anal Chem* 87:10635–10641
- Herm ZR, Bloch ED, Long JR (2014) Hydrocarbon separations in metal-organic frameworks. *Chem Mater* 26:323–338
- Xu J, Xia J, Zhang F, Wang Z (2017) An electrochemical sensor based on metal-organic framework-derived porous carbon with high degree of graphitization for electroanalysis of various substances. *Electrochim Acta* 251:71–80
- Shi L, Chu Z, Dong X, Jin W, Dempsey E (2013) A highly oriented hybrid microarray modified electrode fabricated by a template-free method for ultrasensitive electrochemical DNA recognition. *Nanoscale* 5:10219–10225
- Wang X, Lu X, Wu L, Chen J (2014) 3D metal-organic framework as highly efficient biosensing platform for ultrasensitive and rapid detection of bisphenol a. *Biosens Bioelectron* 65C:295–301
- Morozan A, Moroza F (2012) Metal organic frameworks for electrochemical applications. *Energy Environ Sci* 5:9269–9290
- Xu Z, Yang L, Xu C (2015) Pt@ UiO-66 heterostructures for highly selective detection of hydrogen peroxide with an extended linear range. *Anal Chem* 87:3438–3444
- Novoselov KS, Geim AK, Morozov S, Jiang D, Zhang Y, Dubonos Sa, Grigorieva I, Firsov A (2004) Electric field effect in atomically thin carbon films. *Science (New York, NY)* 306:666–669
- Zheng YY, Li CX, Ding XT, Yang Q, Qi YM, Zhang HM, Qu LT (2017) Detection of dopamine at graphene-ZIF-8 nanocomposite modified electrode. *Chin Chem Lett* 28:1473–1478
- Li Y, Chen Y, Deng DM, Luo LQ, He HB, Wang ZX (2017) Water-dispersible graphene/amphiphilic pyrene derivative nanocomposite: high AuNPs loading capacity for CEA electrochemical immunosensing. *Sensors Actuators B Chem* 248:966–972
- Chen Y, Li Y, Deng DM, He HB, Yan XX, Wang ZX, Fan CH, Luo LQ (2018) Effective immobilization of Au nanoparticles on TiO<sub>2</sub> loaded graphene for a novel sandwich-type immunosensor. *Biosens Bioelectron* 102:301–306
- Mehek R, Iqbal N, Noor T, Nasir H, Mehmood Y, Ahmed S (2017) Novel Co-MOF/graphene oxide electrocatalyst for methanol oxidation. *Electrochim Acta* 255:195–204
- Wang Y, Hou C, Zhang Y, He F, Liu M, Li X (2016) Preparation of graphene nano-sheet bonded pda/mof microcapsules with immobilized glucose oxidase as a mimetic multi-enzyme system for electrochemical sensing of glucose. *J Mater Chem B* 4:3695–3702
- Hong JY, Jung YJ, Park DW, Kim S (2018) Synthesis and electrochemical analysis of electrode prepared from zeolitic imidazolate framework (ZIF)-67/graphene composite for lithium sulfur cells. *Electrochim Acta* 259:1021–1029
- Hummers W, Offeman RE (1958) Preparation of graphitic oxide. *J Am Chem Soc* 80:1339
- Wu R, Qian X, Rui X, Liu H, Yadian B, Zhou K, Wei J, Yan Q, Feng XQ, Long Y, Wang L, Huang Y (2014) Zeolitic imidazolate framework 67-derived high symmetric porous Co<sub>3</sub>O<sub>4</sub> hollow dodecahedra with highly enhanced lithium storage capability. *Small* 10:1932–1938
- Hontoria-Lucas C, Lopez-Peinado A, López-González JDD, Rojas-Cervantes M, Martín-Aranda R (1995) Study of oxygen-containing groups in a series of graphite oxides: physical and chemical characterization. *Carbon* 33:1585–1592
- Lin KYA, Lee WD (2016) Self-assembled magnetic graphene supported ZIF-67 as a recoverable and efficient adsorbent for benzotriazole. *Chem Eng J* 284:1017–1027

31. Gross AF, Sherman E, Vajo JJ (2012) Aqueous room temperature synthesis of cobalt and zinc sodalite zeolitic imidazolate frameworks. *Dalton Trans* 41:5458–5460
32. Taleb M, Ivanov R, Bereznev S, Kazemi SH, Hussainova I (2017) Ultra-sensitive voltammetric simultaneous determination of dopamine, uric acid and ascorbic acid based on a graphene-coated alumina electrode. *Microchim Acta* 184:4603–4610
33. Song H, Xue G, Zhang J, Wang G, Ye BC, Sun S, Tian LP, Li YC (2017) Simultaneous voltammetric determination of dopamine and uric acid using carbon-encapsulated hollow Fe<sub>3</sub>O<sub>4</sub> nanoparticles anchored to an electrode modified with nanosheets of reduced graphene oxide. *Microchim Acta* 184:843–853
34. Kalimuthu P, John SA (2010) Simultaneous determination of ascorbic acid, dopamine, uric acid and xanthine using a nanostructured polymer film modified electrode. *Talanta* 80:1686–1691
35. Chen JC, He P, Bai MH, He SY, Zhang TH, Zhang XQ, Dong FQ (2017) Poly( $\beta$ -cyclodextrin)/carbon quantum dots modified glassy carbon electrode: preparation, characterization and simultaneous electrochemical determination of dopamine, uric acid and tryptophan. *Sensors Actuators B Chem* 252:9–16